

## Overview of the radiometric and biophysical performance of the MODIS vegetation indices

A. Huete<sup>a,\*</sup>, K. Didan<sup>a</sup>, T. Miura<sup>a</sup>, E.P. Rodriguez<sup>a</sup>, X. Gao<sup>a</sup>, L.G. Ferreira<sup>b</sup>

<sup>a</sup>Department of Soil, Water, and Environmental Science, University of Arizona, Tucson, AZ 85721, USA

<sup>b</sup>Universidade Federal de Goiás, Goiânia, GO 74.001-970, Brazil

Received 1 May 2001; received in revised form 4 February 2002; accepted 9 March 2002

### Abstract

We evaluated the initial 12 months of vegetation index product availability from the Moderate Resolution Imaging Spectroradiometer (MODIS) on board the Earth Observing System-Terra platform. Two MODIS vegetation indices (VI), the normalized difference vegetation index (NDVI) and enhanced vegetation index (EVI), are produced at 1-km and 500-m resolutions and 16-day compositing periods. This paper presents an initial analysis of the MODIS NDVI and EVI performance from both radiometric and biophysical perspectives. We utilize a combination of site-intensive and regionally extensive approaches to demonstrate the performance and validity of the two indices. Our results showed a good correspondence between airborne-measured, top-of-canopy reflectances and VI values with those from the MODIS sensor at four intensively measured test sites representing semi-arid grass/shrub, savanna, and tropical forest biomes. Simultaneously derived field biophysical measures also demonstrated the scientific utility of the MODIS VI. Multitemporal profiles of the MODIS VIs over numerous biome types in North and South America well represented their seasonal phenologies. Comparisons of the MODIS-NDVI with the NOAA-14, 1-km AVHRR-NDVI temporal profiles showed that the MODIS-based index performed with higher fidelity. The dynamic range of the MODIS VIs are presented and their sensitivities in discriminating vegetation differences are evaluated in sparse and dense vegetation areas. We found the NDVI to asymptotically saturate in high biomass regions such as in the Amazon while the EVI remained sensitive to canopy variations.

© 2002 Elsevier Science Inc. All rights reserved.

### 1. Introduction

One of the primary interests of the Earth Observing System (EOS) program is to study the role of terrestrial vegetation in large-scale global processes with the goal of understanding how the Earth functions as a system. This requires an understanding of the global distribution of vegetation types as well as their biophysical and structural properties and spatial/temporal variations. Vegetation indices (VIs) are spectral transformations of two or more bands designed to enhance the contribution of vegetation properties and allow reliable spatial and temporal inter-comparisons of terrestrial photosynthetic activity and canopy structural variations. As a simple transformation of spectral bands, they are computed directly without any bias or assumptions regarding land cover class, soil type, or cli-

matic conditions. They allow us to monitor seasonal, inter-annual, and long-term variations of vegetation structural, phenological, and biophysical parameters.

The Moderate Resolution Imaging Spectroradiometer (MODIS) VI products are designed to provide consistent, spatial, and temporal comparisons of global vegetation conditions that can be used to monitor photosynthetic activity (Justice et al., 1998; Running et al., 1994). Two MODIS VIs, the normalized difference vegetation index (NDVI) and enhanced vegetation index (EVI), are produced globally over land at 1-km and 500-m resolutions and 16-day compositing periods. Whereas the NDVI is chlorophyll sensitive, the EVI is more responsive to canopy structural variations, including leaf area index (LAI), canopy type, plant physiognomy, and canopy architecture (Gao, Huete, Ni, & Miura, 2000). The two VIs complement each other in global vegetation studies and improve upon the detection of vegetation changes and extraction of canopy biophysical parameters.

The MODIS NDVI is referred to as the “continuity index” to the existing 20+ year NOAA-AVHRR-derived NDVI time

\* Corresponding author. Tel.: +1-520-621-3228; fax: +1-520-621-1791.  
E-mail address: ahuete@ag.arizona.edu (A. Huete).

series, which could be extended by MODIS data to provide a longer-term data record for use in operational monitoring studies. The AVHRR-NDVI has been widely used in various operational applications, including famine early warning systems, land cover classification, health and epidemiology, drought detection, land degradation, deforestation, change detection and monitoring (Cihlar et al., 1997; Goward, Markham, Dye, Dulaney, & Yang, 1991; Tucker, Townshend, & Goff, 1985). The NDVI is also an important parameter to various kinds of local, regional, and global scale models, including general circulation and biogeochemical models (Peterson et al., 1988; Potter, Klooster, & Brooks, 1999). They serve as intermediaries in the assessment of various biophysical parameters, such as green cover, biomass, LAI, and fraction of absorbed photosynthetically active radiation (fAPAR) (Asrar, Fuchs, Kanemasu, & Hatfield, 1984; Sellers, 1985; Tucker, 1979). The AVHRR-NDVI time series has been successfully used in many studies on the interannual variability of global vegetation activity and in relating large-scale interannual variations in vegetation to climate (Myneni, Keeling, Tucker, Asrar, & Nemani, 1997).

The normalized difference vegetation index (NDVI) is a normalized ratio of the NIR and red bands,

$$\text{NDVI} = \frac{\rho_{\text{NIR}} - \rho_{\text{red}}}{\rho_{\text{NIR}} + \rho_{\text{red}}} \quad (1)$$

where  $\rho_{\text{NIR}}$  and  $\rho_{\text{red}}$  are the surface bidirectional reflectance factors for their respective MODIS bands. The NDVI is successful as a vegetation measure in that it is sufficiently stable to permit meaningful comparisons of seasonal and inter-annual changes in vegetation growth and activity. The strength of the NDVI is in its ratioing concept, which reduces many forms of multiplicative noise (illumination differences, cloud shadows, atmospheric attenuation, certain topographic variations) present in multiple bands. The NDVI is functionally equivalent to the simple ratio (SR = NIR/red) such that  $\text{NDVI} = (\text{SR} - 1) / (\text{SR} + 1)$ . The main disadvantage of the NDVI is the inherent nonlinearity of ratio-based indices and the influence of additive noise effects, such as atmospheric path radiances. The NDVI also exhibits scaling problems, asymptotic (saturated) signals over high biomass conditions, and is very sensitive to canopy background variations with NDVI degradation particularly strong with higher canopy background brightness (Huete, 1988).

Non-ratioing vegetation indices such as the perpendicular vegetation index (PVI) and the green vegetation index (GVI) are generally more linear with less saturation problems, but require external and sensor noise removal in the derivation of surface reflectances that are input to VI computation (Crist & Cicone, 1984; Richardson & Wiegand, 1977). Current emphasis in the EOS era involves operational ‘external’ noise removal through improved calibration, atmospheric correction, cloud and cloud shadow removal, and standardization of sun-surface-sensor geometries with bidirectional reflectance distribution function (BRDF) models. This minimizes the

need for ‘ratioing-based’ indices and allows for the introduction of alternative and enhanced vegetation indices for operational monitoring of the Earth’s vegetation (Verstraete & Pinty, 1996). The enhanced vegetation index (EVI) was developed to optimize the vegetation signal with improved sensitivity in high biomass regions and improved vegetation monitoring through a de-coupling of the canopy background signal and a reduction in atmosphere influences. The equation takes the form,

$$\text{EVI} = G \frac{\rho_{\text{NIR}} - \rho_{\text{red}}}{\rho_{\text{NIR}} + C_1 \times \rho_{\text{red}} - C_2 \times \rho_{\text{blue}} + L} \quad (2)$$

where  $\rho$  are atmospherically corrected or partially atmosphere corrected (Rayleigh and ozone absorption) surface reflectances,  $L$  is the canopy background adjustment that addresses nonlinear, differential NIR and red radiant transfer through a canopy, and  $C_1$ ,  $C_2$  are the coefficients of the aerosol resistance term, which uses the blue band to correct for aerosol influences in the red band. The coefficients adopted in the EVI algorithm are,  $L=1$ ,  $C_1=6$ ,  $C_2=7.5$ , and  $G$  (gain factor) = 2.5 (Huete, Justice, & Liu, 1994; Huete, Liu, Batchily, & van Leeuwen, 1997).

The “atmospheric resistance” concept is based on the wavelength dependency of aerosol effects, utilizing the more atmosphere-sensitive blue band to correct the red band for aerosol influences (Kaufman & Tanré, 1992). The objective is to find a function,  $f_{\lambda}(\rho_{\lambda}, \rho_{\text{blue}} - \rho_{\text{red}})$ , that is stable against variations of atmospheric aerosol condition. The EVI was found to perform well in the heavy aerosol, biomass burning conditions in Brazil (Miura, Huete, van Leeuwen, & Didan, 1998). Later, Miura, Huete, Yoshioka, and Holben (2001) showed the atmosphere-resistant VIs to successfully minimize residual aerosol effects resulting from the dark target-based atmospheric correction (DTAC) approach utilized in the MODIS surface reflectance products (Vermote, El Saleous, & Justice, 2002, this issue). The DTAC-derived surface reflectances are subject to errors due to the assumptions and characteristics of the algorithm, with the main source of uncertainty associated with the assumed or estimated DT surface reflectance. Other errors are due to the spatial heterogeneity of aerosol optical thickness since coarse grid-based corrections are often applied. Miura et al. (2001) found that these errors preserve the wavelength dependency of aerosol effects such that the atmosphere resistance concept could still be applied with improved results to the MODIS EVI.

The canopy background correction is relevant for vegetation monitoring since 70% of the Earth’s terrestrial surface consists of open canopies with significant canopy background signals exerting some effect on the canopy reflectance properties (Graetz, 1990). These open canopies include deserts, tundra, grasslands, shrublands, savannas, woodlands, wetlands, and many open forested areas. Canopy backgrounds include a wide variety of weathered geologic substrates, leaf litter, water, and snow. Canopy background noise

is most severe at intermediate levels of vegetation (40–60% cover) since it is the ‘coupled’ influence of the canopy background and transmittance properties of the overlying canopy that determine the extent of noise in the VIs. This ‘background’ influence must be removed in order to better interpret spatial and temporal variations associated with vegetation from variations associated with the canopy background. The fundamental objective of vegetation indices is to isolate the ‘green’, photosynthetically active signal from the spatially and temporally variable ‘mixed’ pixels, to allow meaningful spatial and temporal intercomparisons of vegetation activity.

In this paper, we describe the status of the MODIS VI products and analyze their performance over the first 12 months of MODIS instrument operation. The MODIS VIs were evaluated as to their ability to monitor and assess

vegetation conditions over a diverse range of biomes. Site intensive comparisons were made at four validation test sites utilizing low altitude, aerial reflectance measurements and field-based biophysical measurements. Comparisons were also made between the MODIS VI products and the NDVI product from the NOAA-14 AVHRR sensor. The objective was to demonstrate the performance and validity of the MODIS VI products over various biome types and to assess their capability for vegetation change detection and biophysical parameter retrievals.

**2. MODIS VI product (algorithm) description**

The MODIS standard VI products include two, gridded vegetation indices (NDVI, EVI) and quality analysis (QA)

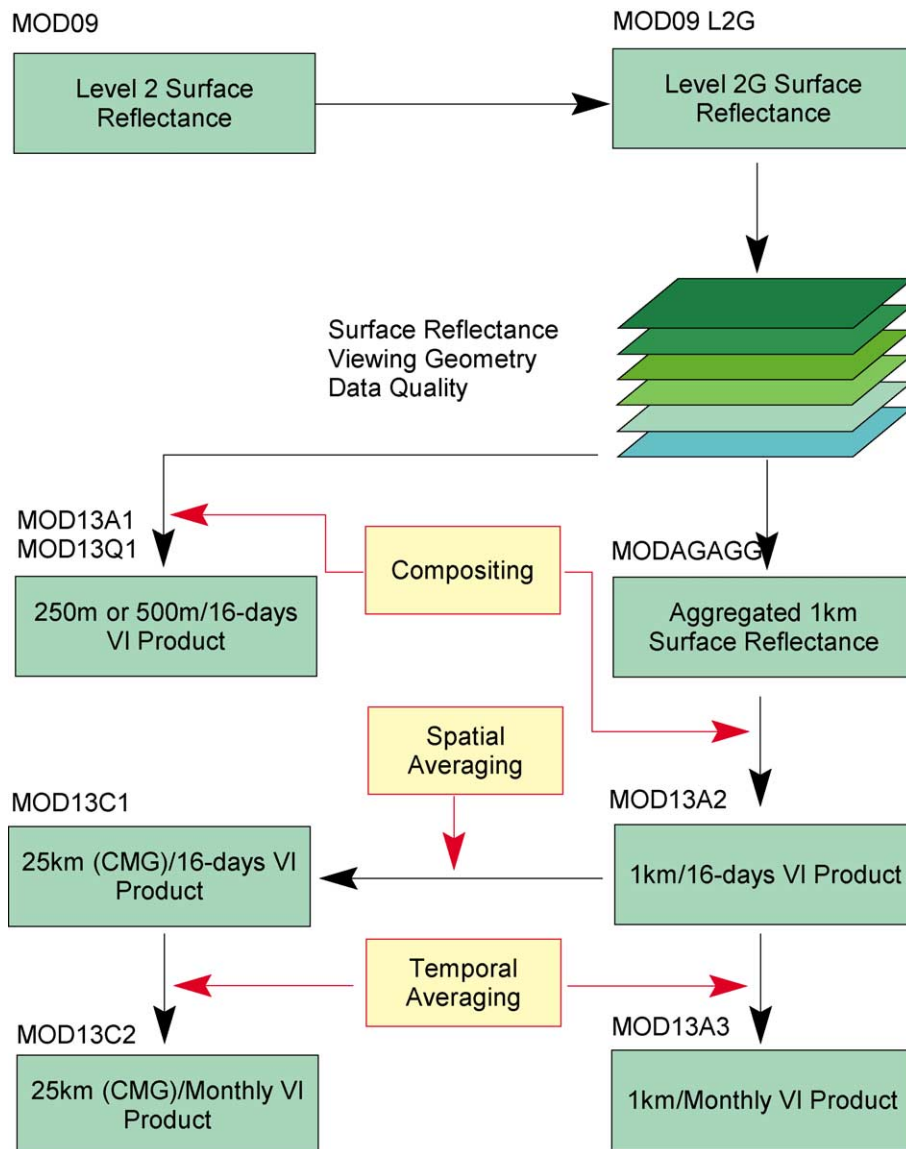


Fig. 1. Flow diagram of MODIS VI products.

with statistical data that indicate the quality of the VI product and input reflectance data. They are currently produced at 16-day intervals at 500-m and 1-km resolutions with limited production at 250-m resolution. A coarser, climate modeling grid (CMG) version of the VI products at a resolution of 25 km is also in development, as are monthly versions of all the VI products (Fig. 1). The products are labeled as:

- MOD13A1: 16-day 500-m VI (high resolution/globally produced)
- MOD13Q1: 16-day 250-m VI (high resolution/limited production)
- MOD13A2: 16-day 1-km VI (standard resolution/globally produced)
- MOD13A3: Monthly 1-km VI (standard resolution/globally produced)
- MOD13C1: 16-day 25-km VI (coarse resolution (CMG)/globally produced)
- MOD13C2: Monthly 25-km VI (coarse resolution (CMG)/globally produced)

For production purposes the MODIS VIs are output in tile units that are approximately 1200 by 1200 km in the integerized sinusoidal (ISIN) grid projection. When mosaicked, all tiles cover the terrestrial Earth and the MODIS VI can be generated globally each 16 days. The VI products rely on the level 2 daily surface reflectance product (MOD09 series), which are corrected for molecular scattering, ozone absorption, and aerosols (Vermote, et al., 2002, this issue). The VI algorithms ingest the level 2G (gridded) surface reflectances and temporally composite these to generate the 16-day, 250/500 m or 1-km VI products (Fig. 1). The 1-km VI product (MOD13A2), however, requires aggregation of 250- and 500-m MODIS pixel sizes to 1 km by way of the ‘MODAGAGG’ algo-

rithm. The VI output file contains a variable number of ‘Science Data Sets’ (SDS) that include the 16-day NDVI and EVI values; the 16-day QA for NDVI and EVI; the residual red (band 1), near-infrared (band 2), middle-infrared (band 6), and blue (band 3) reflectances; and view zenith, solar zenith, and relative azimuthal angles from the selected, composited pixels. There is some production of the 250-m MODIS VI products (MOD13Q1) over a limited set of tiles. The 250-m EVI currently uses a disaggregated 500-m blue band for aerosol resistance. The 250-m VI products are planned to be in full production and globally available.

The MODIS VI algorithm operates on a per-pixel basis and relies on multiple observations over a 16-day period to generate a composited VI. Due to sensor orbit overlap and multiple observations in a single day, a maximum of 64 observations over a 16-day cycle may be collected; however, due to the presence of clouds and actual sensor spatial coverage, this number will range between 0 and 64 with fewer observations near equatorial latitudes. Once all 16 days of observations are collected, the MODIS VI algorithm applies a filter to the data based on quality, cloud, and viewing geometry (Fig. 2). Only the higher quality, cloud-free, filtered data are retained for compositing. Cloud-contaminated pixels and extreme off-nadir sensor view angles are considered lower quality while cloud-free and nadir-view pixels with minimal residual atmospheric aerosols represent the best quality pixels (van Leeuwen, Huete, & Laing, 1999). MODIS is a whiskbroom sensor that causes the pixel size to increase with scan angle by as much as a factor of four. Nadir-view pixels possess minimal distortions and match the extensive set of spaceborne (e.g. Landsat), airborne (e.g. AVIRIS), and ground-based field measurements routinely made at nadir-view throughout terrestrial surfaces. The number of acceptable pixels over a 16-day compositing period is thus, further reduced and is typically less than 10 and often less than 5,

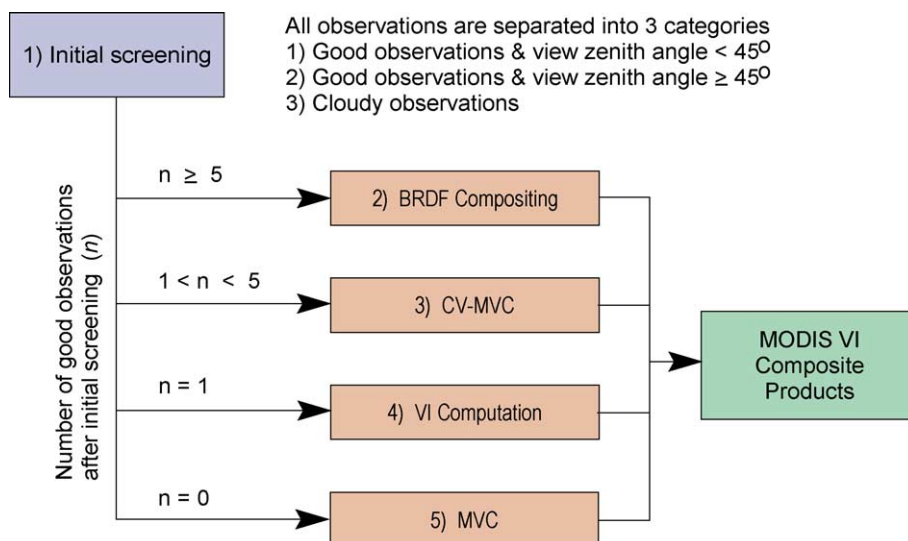


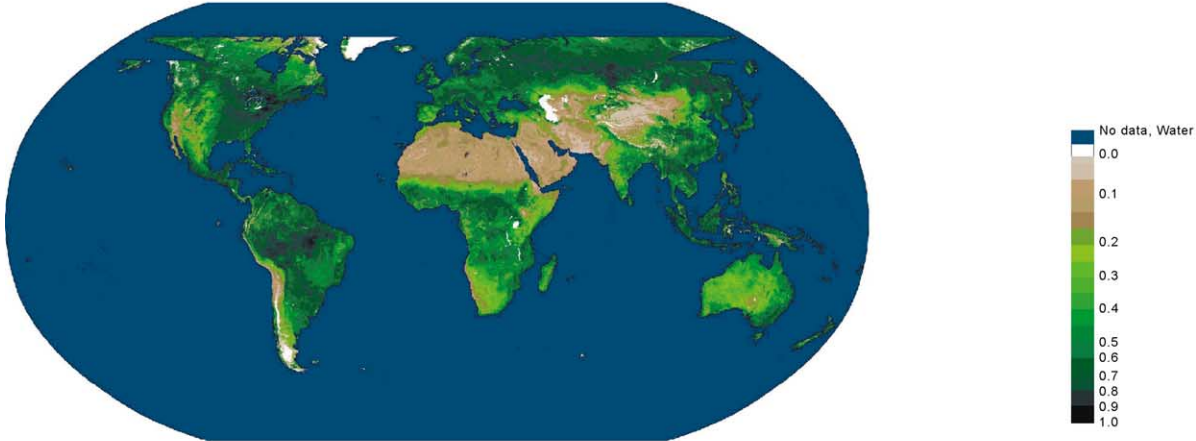
Fig. 2. Diagram of MODIS VI compositing methodology.

especially when one considers a mean global cloud cover of 50–60%.

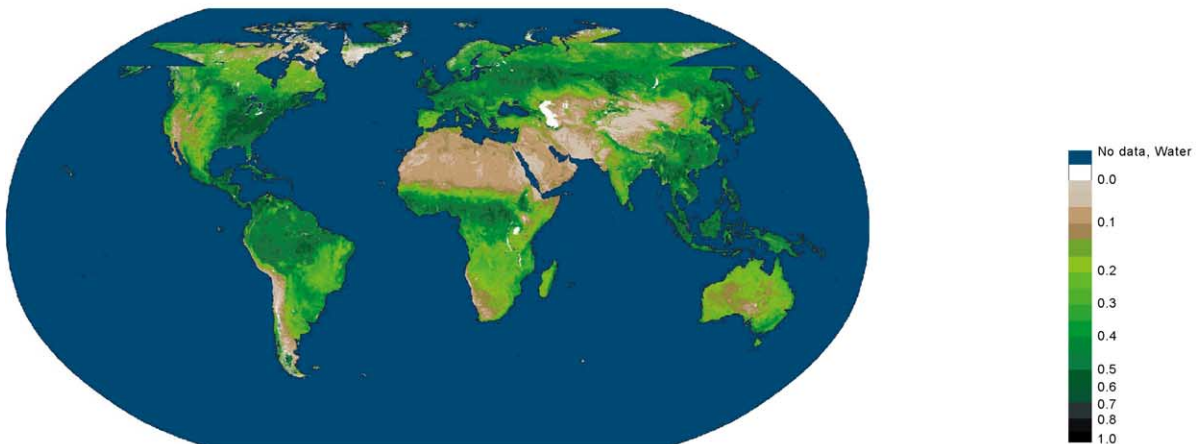
The goal of compositing methodologies is to select the best observation, on a per pixel basis, from all the retained filtered data, to represent each pixel over the 16-day

compositing period. The methodology should provide spatial and temporal consistency in VI values on an operational basis and be consistent with the goals of developing a long-term time series of VI values such that no biases detrimental to the time series record are introduced (Roderick, Smith, &

### NDVI Composite, June 25<sup>th</sup>-July 10<sup>th</sup>, 2000



### EVI Composite, October 15<sup>th</sup>-October 30<sup>th</sup>, 2000



### EVI QA, October 15<sup>th</sup>-October 30<sup>th</sup>, 2000

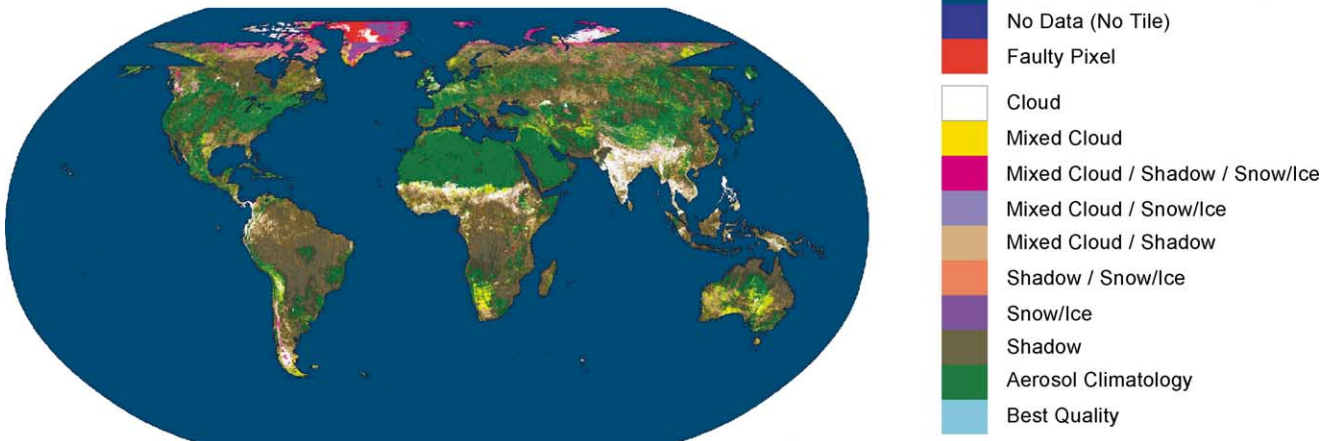


Fig. 3. Example of 1-km, 16-day composited MODIS NDVI and EVI products and an EVI QA image.

Lodwick, 1996). The MODIS VI compositing algorithm consists of three components (Fig. 2):

- BRDF-C: bidirectional reflectance distribution function composite,
- CV-MVC: constrained-view angle-maximum value composite,
- MVC: maximum value composite.

The technique employed depends on the number and quality of observations. The maximum value composite (MVC) is similar to that used in the NOAA AVHRR-NDVI (Pathfinder) product, in which the pixel observation with the highest NDVI value is selected to represent the compositing period (16 days). The MVC method is an efficient method of compositing when applied to AVHRR-NDVI data that is not corrected for atmosphere (Holben, 1986). The method minimizes the selection of cloudy and heavy aerosol pixels and sensor view angle influences are not as strong in pixels uncorrected for atmosphere (Cihlar, Manak, & Voisin, 1994). Many studies, however, have shown the MVC method to select pixels with large view and solar zenith angles, which may not always be cloud-free (Cihlar et al., 1997; Goward, et al., 1991). Pixels from off-nadir views in the forward scatter direction and under clear atmosphere conditions are preferentially selected due to the strong anisotropy of many vegetated surfaces (Kimes, 1983). The MVC approach thus generally selects pixels with NDVI values greater than the nadir value.

In the MODIS case, surface anisotropy effects are more pronounced since reflectance values are atmospherically corrected prior to compositing and VI computation. The MVC method, in this case, will dramatically increase the selection of off-nadir pixels, particularly over open canopies, which exhibit higher NDVI values when viewed obliquely. The CV-MVC and BRDF compositing techniques are designed to constrain the strong angular variations encountered in the MVC selection method. The CV-MVC compares the two highest NDVI values and selects the observation closest to nadir view to represent the 16-day composite cycle. This helps to reduce spatial and temporal discontinuities in the composited product. Both the NDVI and EVI are computed using the same pixel observation, i.e., there is no separate maximum EVI methodology.

The BRDF scheme is a more elaborate and constrained technique in which all bidirectional reflectance observations, of acceptable quality, are utilized to interpolate to their nadir-equivalent band reflectance values from which the VI is computed and produced. The Walthall semi-empirical BRDF model is utilized for the BRDF inversion scheme,

$$\rho_{\lambda}(\theta_v, \phi_s, \phi_v) = a_{\lambda}\theta_v^2 + b_{\lambda}\theta_v\cos(\phi_v - \phi_s) + c_{\lambda}, \quad (3)$$

where  $\rho_{\lambda}$  is the atmospherically corrected reflectance in band  $\lambda$ ,  $\theta_v$  is the satellite view zenith angle,  $\phi_v$  is the

satellite view azimuth angle,  $\phi_s$  is the solar azimuth angle, and  $a_{\lambda}$ ,  $b_{\lambda}$ ,  $c_{\lambda}$  are the model parameter coefficients (Walthall, Norman, Welles, Campbell, & Blad, 1985). The model is fitted to the observations by a least squares procedure on a per-pixel basis to estimate nadir view equivalent reflectance values ( $c_{\lambda}$ ). At least five good quality observations ( $\theta_v \leq 45^\circ$ ), after the initial screening process, are required for model inversion. The fitting results are considered to be satisfactory if the interpolated reflectance values ( $c_{\lambda}$ ) are within a range specified by the MVC-selected NDVI. If there are less than five acceptable values, then the CV-MVC module is employed. If only one good observation is available, then the VIs are computed from this observation. If no observations pass the initial data screening, then the MVC technique is used as the final backup to the BRDF and CV-MVC schemes such that the highest NDVI pixel is selected, regardless of data quality, to complete a composite image.

The BRDF composite scheme has the disadvantage of not only requiring five clear pixels, but is also highly dependent on the accuracy of the cloud mask. Since the nadir equivalent value is interpolated from five or more pixels, one contaminated (residual cloud) pixel will compromise the final computed nadir value. Unfortunately, vegetation is most active when clouds (rainfall) are most prevalent and this limits the geographic extent of the BRDF inversion procedure to dry periods and areas with low cloud cover. As a result, the BRDF module is currently turned off until a more thorough analysis and evaluation of its utility can be completed. The MODIS VI products also appear to be significantly affected by the presence of snow, such that NDVI values are reduced while EVI values increase. The EVI algorithm uses the soil-adjusted vegetation index (SAVI) as a snow quality check. The SAVI and EVI are highly correlated with small variations due to aerosols and large deviations associated with snow. When the two indices strongly deviate, the algorithm switches to a SAVI-derived value for the EVI. An example of the 16-day, 1-km composited NDVI and EVI products along with an EVI QA image is shown in Fig. 3.

### 3. Methods

To evaluate the performance of the MODIS VI products, we utilized airborne radiometric measurements, higher resolution Landsat ETM+ imagery, and in situ field biophysical data collected over four validation test sites representing a variety of land surface biome types (Table 1). The test sites were large enough to permit reasonable MODIS coverage yet small enough to enable a sufficient number of independent field observations. Independent retrievals of surface reflectances and VIs were made with the MODLAND Quick Airborne Looks (MQUALS) package consisting of a calibrated and traceable “transfer radiometer”, an array of digital spectral cameras, and GPS, all

Table 1  
MODIS and MQUALS data collection at the validation sites

Site name	MQUALS campaign (DOY)	MQUALS solar zenith angle	500-m, MODA1 16-day composite data (DOY)	MODIS solar zenith angle	MODIS view zenith angle
Walnut Gulch Experimental Watershed, Arizona, USA	March 31, 2000 (091)	29	March 21–April 5 (081–096)	30	+ 19.5
La Jornada Experimental Range, New Mexico, USA	May 9, 2000 (130)	30	May 8–May 23 (129–144)	14	+ 40 and 0 <sup>a</sup>
Brasilia National Park, Brasilia, Brazil	May 5 and July 9, 2000 (126, 191)	45	April 22–May 7 (113–128)	37	+ 13
Tapajós National Forest, Santarem, Brazil	July 9, 2000 (191)	29	June 25–July 10 (177–192)	34	– 19.5

<sup>a</sup> Single day, nadir view image.

connected to a laptop computer with Labview software for synchronized measurements (Huete et al., 1999). Independent measurements are necessary to assess how well the MODIS VI products represent actual surface conditions as well as to analyze where the uncertainties in the VI products lie and identify systematic errors. Errors associated with MODIS sensor calibration, instrument noise, atmosphere correction, and cloud masking will propagate into the final product. The goal of validation is to demonstrate how well MODIS products are able to depict temporal and spatial variability in vegetation properties and condition (Justice et al., 2000).

An Exotech radiometer with four spectral MODIS bands co-aligned to within  $\pm 0.5^\circ$  was flown at two of the sites, while an ASD spectroradiometer with continuous spectral sampling from 370 to 1050 nm with 3.5-nm spectral resolution was flown at two other sites (Table 2). All sites were flown at 150- to 300-m AGL with negligible atmosphere influences. The ground component of the field campaigns consisted of a Spectralon reference panel with a second, cross-calibrated radiometer mounted for continuous measurements of site irradiance. At the Walnut Gulch and Jornada sites, we also conducted ground-based yoke transects of 1-km length with Exotech and ASD radiometers from a height of 2 m and field of view of  $15^\circ$ . At all sites,

we carried out a limited set of biophysical measurements involving plant and leaf area index (PAI/LAI) and percent green cover (Table 3). There was some difficulty in matching limited ground biophysical samplings data with MODIS pixels, particularly when each biome type presented a unique challenge in measuring PAI/LAI values. PAI values of forest, shrub, and woodland areas were estimated with a plant canopy analyzer (LAI-2000, Licor), while green LAI of the grass areas involved some destructive sampling. Percent green cover at all sites were measured with point sampling frames and photographs.

Four Landsat ETM+ scenes were acquired over the Jornada site for the 2000 growing season. These were atmospherically corrected using the '6S' radiative transfer code and sun photometer measurements. The 16-day MODIS VI composites were processed, geolocated, and co-registered to the field-and airborne data collected over the four test sites (Table 1). The VI composites were based on atmospherically corrected surface reflectances (MOD 09) with aerosol correction based on coarse-grid climatology. Approximately 10–20, 500-m MODIS pixels at each site were averaged and compared with the aggregated reflectances from the MQUALS data sets. With the BRDF module turned off, the CV-MVC approach, based on NDVI values, was utilized for compositing in this study.

### 3.1. Site descriptions

The Walnut Gulch Experimental Watershed is a USDA research station, located in the fringes of the Sonoran desert in southeastern Arizona. The area encompasses 145 km<sup>2</sup> in a high foothill alluvial fan portion of the San Pedro Watershed. This site was once covered by grassland but shrubs now dominate two thirds of the watershed. Grazing is the predominant land use. The Jornada Experimental Range is

Table 2  
Spectral characteristics of MQUALS components

Filter/sensor	MODIS sensor	Exotech radiometer	ASD (convoluted)
Channel 1, red	620–670 nm	623–670 nm	620–670 nm
Channel 2, NIR	841–876	838–876	841–876
Channel 3, blue	459–479	456–475	459–479
Channel 4, green	545–565	544–564	545–565

Table 3  
Validation site descriptions

Site name	Lat./Long.	Biome type	PAI/%cover	Mean annual precipitation (mm)	Mean annual temperature (°C)	Elevation (m)
Walnut Gulch Experimental Watershed, Arizona USA	Lat. 31.74 Long. - 109.85	Sonoran semi-arid grass/shrub	1 0–20	324	15.8	1190–2150
Jornada Experimental Range, New Mexico USA	Lat. 32.61 Long. - 106.87	Chihuahuan semi-arid grass/shrub	0.5 0–11	210	15.2	1180–1375
Brasilia National Park, Brasilia Brazil	Lat. - 15.58 Long. - 48.0	Cerrado grassland and woodland	3–5 40–60	1600	22	1100–1300
Tapajos National Forest, Santarém Brazil	Lat. - 2.86 Long. - 54.96	Tropical Broadleaf Forest	5–7 >90	2180	27	80–110

located in the northern Chihuahuan desert, 40 km north of Las Cruces, New Mexico and encompasses 78 km<sup>2</sup>. This site is part of the NSF Long-Term Ecological Research (LTER) network, where there has been a well-documented land cover shift from semi-desert perennial grassland to desert shrubland (Schlesinger, Reynolds, & Cunningham, 1990).

The Brasilia National Park (BNP) site consists of 300 km<sup>2</sup> of protected savanna near Brasilia. This site is the largest ‘Large Scale Biosphere-Atmosphere Experiment in Amazonia’ (LBA) site in the cerrado region of Brazil, encompassing all the common savanna formations. Land cover subtypes include the transitions from the dominant herbaceous stratum (savanna grassland and shrub savanna) to the more complex, wood-dominated stratum (wooded savanna and the savanna woodland). The Tapajos National Forest site is an LBA core site in the seasonal tropical humid broadleaf forest south of Santarém, Brazil. This site encompasses a range of primary forest, pasture, and forest regeneration and is indicative of the largest biome type in South America. At the four sites, mean annual rainfall ranged from 200 mm (Jornada) to >2000 mm (Tapajos) with associated green covers from <10% to >90% (Table 3).

In addition to the four field campaigns, we also extracted 16-day MODIS VI and reflectances over additional test validation sites, mostly in North and South America during the 12-month period. This included the Harvard Forest, Konza Prairie, and Seville LTER sites in Massachusetts, Kansas, and New Mexico, respectively (see [www.lternet.edu](http://www.lternet.edu)) and a needleleaf forest site in the Cascades, Oregon. The MODIS VI products were also analyzed over a few hyperarid sites, devoid of vegetation in order to investigate the zero baseline of VI values. This included an Atacama desert site in northern Chile and Uyuni Salt Flats, a high altitude desert site in the Bolivian altiplano. The North American test sites were also co-registered with a seasonal

set of 1-km AVHRR NDVI values from the NOAA-14 sensor (James & Kalluri, 1994).

## 4. Results

### 4.1. Radiometric comparisons

A comparison of MODIS nadir-view data (single day) with coincident MQUALS data provides an assessment of how well the VI products are performing prior to temporal compositing. Of the four sites flown with MQUALS, we were only successful in obtaining coincident, cloud-free, nadir-view MODIS imagery at the semiarid Jornada site on May 9, 2000 (Fig. 4). The MODIS and MQUALS reflectances and VIs matched fairly well over the three land cover types within the Jornada site with MODIS blue, red, and NIR reflectances slightly higher than those acquired directly over the canopy with MQUALS. This resulted in the MODIS NDVI values being slightly lower than the MQUALS NDVI values while the EVI values were identical in both sets of observations. During this period, the MODIS VI products were derived from surface reflectances based on coarse-grid climatology aerosol corrections and thus, were not atmospherically corrected on a per-pixel basis. The MODIS VI products were able to distinguish among the three main land cover types (creosotebush, grass, and transition) present at the Jornada site.

The overall test of performance is to compare the 16-day composite MODIS VI products with the MQUALS top-of-canopy, nadir-view reflectances, and VI values. The composited products have the primary goal of generating cloud-free maps of vegetation activity while attempting to approximate nadir-view vegetation conditions. The MODIS composited products inevitably possess a wide distribution of view angles with some residual atmospheric and cloud effects, and thus aggregate all the uncertainties involved in the compositing

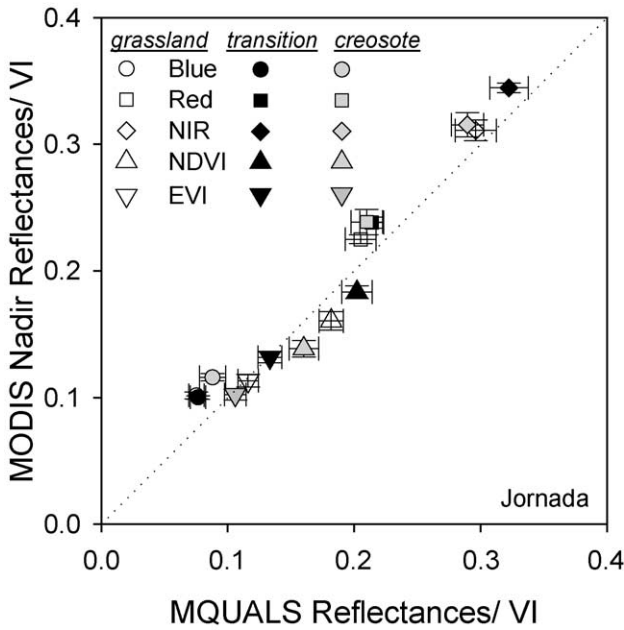


Fig. 4. Comparison of single day, nadir view MODIS data (500 m) with MQUALS data for the Jornada site on May 9, 2000.

routine and atmosphere correction process. The 16-day MODIS reflectance and VI composites compared quite well with the MQUALS-derived validation data over the four sites encompassing semiarid to humid forest vegetation (Fig. 5). There is a good correspondence between the two sets of reflectances with the blue values showing the poorest agreement and the red showing the best match. This indicates that the compositing procedure, with its inherent angular and atmosphere variations, was able to estimate the nadir-view, top-of-canopy reflectances well. The greatest deviation oc-

curred with the NIR reflectances at the Tapajos tropical forest site where there were persistent, residual cloud and cloud shadow contamination problems.

The composited VIs matched fairly well with their nadir-based and atmosphere-free MQUALS counterpart despite the off-nadir MODIS observations and cloud/cloud shadow contamination (Fig. 5b). The composited MODIS data over the four sites resulted in view angles ranging from  $-20^\circ$  (backscatter) to  $+40^\circ$  (forward scatter) and solar zenith angles from  $14^\circ$  to  $37^\circ$  (Table 1). The nadir-view MQUALS data had solar zenith angles between  $29^\circ$  and  $45^\circ$ . The MODIS VI values were slightly higher than the MQUALS data, except for the Tapajos site. The lowest VI values were found over the two semi-arid sites (Jornada and Walnut Gulch) while the highest values were from the Tapajos forest site. The three cerrado land cover sites in the active growing season had intermediate VI values.

A multitemporal data set of MODIS 16-day, 500-m VI composites for the 2000 growing season was extracted over the relatively homogeneous grassland site at Jornada and compared with four ETM+ acquisitions, five single-day (nadir-view) MODIS images, and four ground-based transect measurements (Fig. 6). All data sets (ground, MQUALS, ETM+, MODIS) are in good agreement with each other with the exception of the MODIS EVI composite, DOY 161–176, and the MODIS NDVI composite, DOY 273–288, which deviated from their equivalent ETM+ derived VI values. There was a crucial, peak of the growing season, composite period missing (DOY 209–224) due to a reset of the MODIS instrument. The acquired ETM+ image on DOY 210 confirmed that the peak of the growing season was over and the vegetation had started its dry-down phase (Fig. 6). The NDVI values were consistently higher than those of the EVI; however, the overall contrast between dry and wet

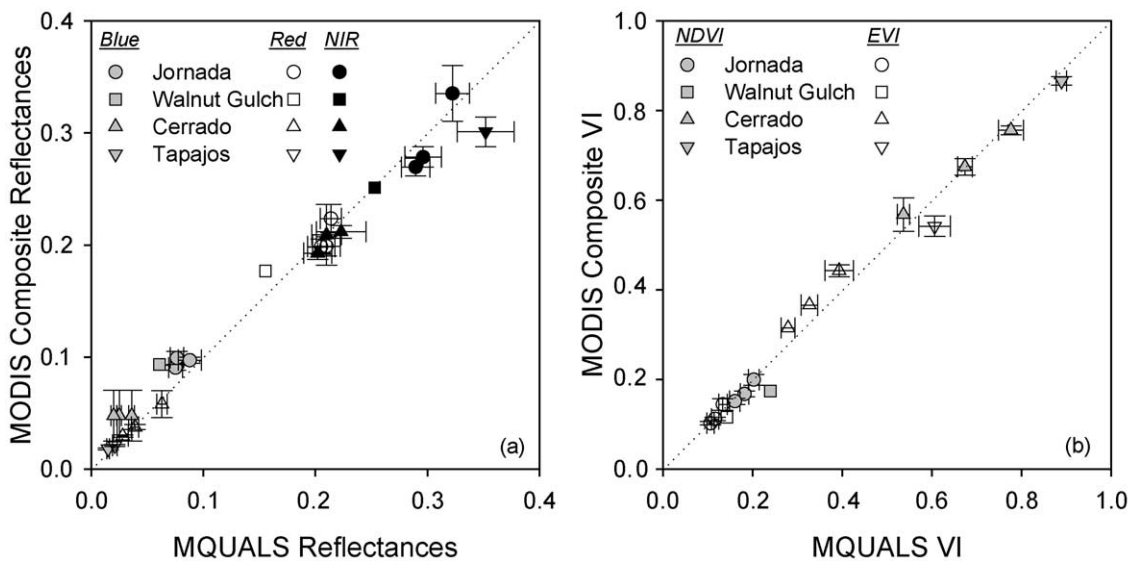


Fig. 5. Comparisons of (a) 500 m, 16-day composited MODIS reflectances and (b) 500 m, 16-day composited MODIS VIs with top-of-canopy MQUALS reflectances and VIs for the four validation test sites.

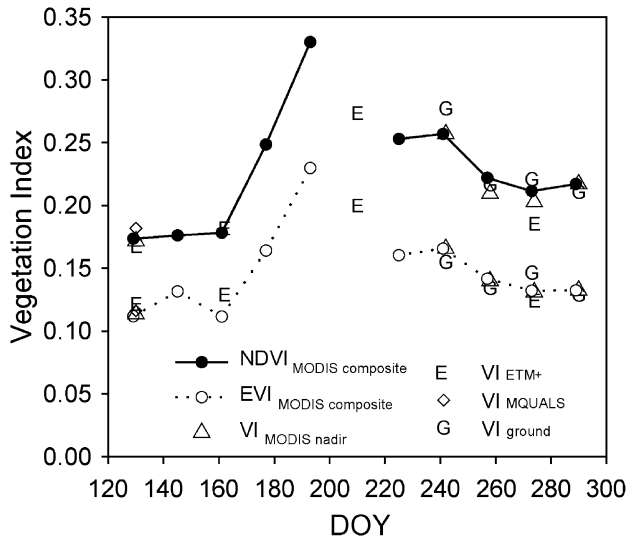


Fig. 6. Multitemporal profile comparisons of 500 m MODIS composited NDVI and EVI data with MQUALS, Landsat ETM+, and radiometric field data.

seasons was similar (0.17 to 0.33 for the NDVI and 0.09 to 0.23 for the EVI). EVI values are generally lower in order to avoid saturation in high biomass areas.

4.2. Multitemporal (seasonal) vegetation profiles

Multitemporal extracts of 1-km, 16-day MODIS VI composites were made over a range of validation test sites to assess MODIS capability to depict phenology and seasonal variations in vegetation activity (Figs. 7–11). The MODIS VI composited products include four MODIS band reflectances (bands 1, 2, 3, and 6) and the sun and view angle geometry, corresponding to the selected pixel over the composite period. This is useful in interpreting the seasonal

VI profiles and allows for the calculation of additional VIs, such as smoke-resistant, middle-infrared (MIR)-based VIs. Missing composite periods, due to MODIS instrument and production related difficulties, are displayed with broken lines. The seasonality of the broadleaf, eastern deciduous Harvard Forest site as depicted by the MODIS VIs are shown in Fig. 7. This site has an annual precipitation amount of ~2800 mm and an LAI of approximately 4 during the growing season. There are also evergreen, conifer plantations present at the site. Both the NDVI and EVI show the growing season commencing in April and maximum green foliage over the months from May through September (Fig. 7). There appeared to be more erratic, view angle variations in the NDVI in the first half of the growing season with much less variations during the dry down phase starting in October. The EVI values exhibited a smoother, more symmetrical seasonal profile with a narrower, well-defined peak greenness period (Fig. 7). The NDVI responds similarly to broadleaf and needleleaf forests and hence the dry-down phase is more gradual as the broadleaf canopy loses its leaves and the needleleaf forest canopy remains green. On the other hand, the EVI is very sensitive to needleleaf/broadleaf canopy structures with EVI values over needleleaf forests approximately one-half those over broadleaf forests resulting in sharper contrasts between the two forest types and a more pronounced broadleaf dry-down phase.

The red, blue, and MIR bands are fairly stable most of the year with MIR values slightly higher than the red and blue bands, particularly in the dry season. Only the NIR band showed a strong seasonal variation with the highest values during the peak growing season, essentially mimicking the EVI temporal response curve. From January through March 2001, there were snow problems that affected both MODIS VI products (Fig. 7). The snow can be observed with the increased red, blue, and NIR reflectances concur-

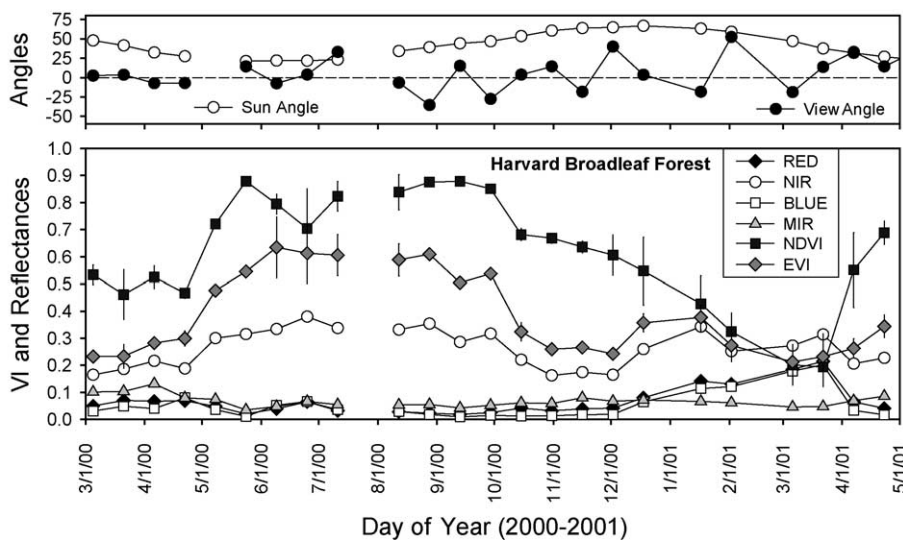


Fig. 7. 1-km MODIS VI and reflectance seasonal profiles, with view and sun angle variability of the selected pixels, at the Harvard Forest site.

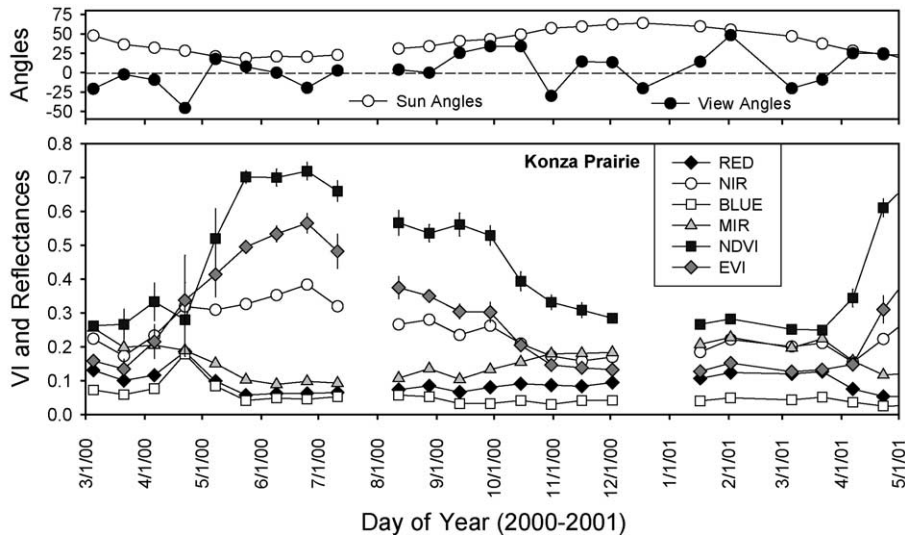


Fig. 8. 1-km MODIS VI and reflectance seasonal profiles, with view and sun angle variability of the selected pixels, at the Konza Prairie site.

rent with low MIR reflectances. The presence of snow caused the NDVI values to decrease dramatically due to canopy background brightness influences. The forest NDVI signal is restored with the snow melting in April. In contrast, the snow background caused a false positive signal in the EVI, a problem that is being resolved through the use of the SAVI.

The two indices similarly depicted differences in the initiation of green-up as well as the peak of the growing season for the Konza Prairie site (Fig. 8). This native tallgrass prairie has an annual rainfall of ~800 mm and an LAI of 2–3 during the peak of the growing season. The peak of the growing season occurred in June and appeared broader in the NDVI temporal profile starting as early as May 18 and ending as late as the end of June. The red, blue, and MIR curves exhibited more variation than found at the

Harvard Forest site but follow the same trend with the MIR higher than the red and blue, particularly as the grass undergoes senescence. The MIR band exhibited a significant seasonal trend with higher values in the winter period. Once again, the NIR reflectances traced out the growing season dynamics fairly well, while the red band showed lower sensitivity to temporal seasonal dynamics. View angle variations were generally lower ( $\pm 30^\circ$ ) than encountered at the Harvard Forest site; however, there was one anomalous reflectance peak around mid-April 2000 that corresponded to a strong backscatter view angle selection ( $-40^\circ$ ), which caused the NDVI to decrease.

Very strong VI seasonal profiles were still observed over the semi-arid grass/shrub site at Walnut Gulch (Fig. 9). LAI values were less than 1 as annual rainfall is only ~300 mm. Both indices were similar in their depiction of the important

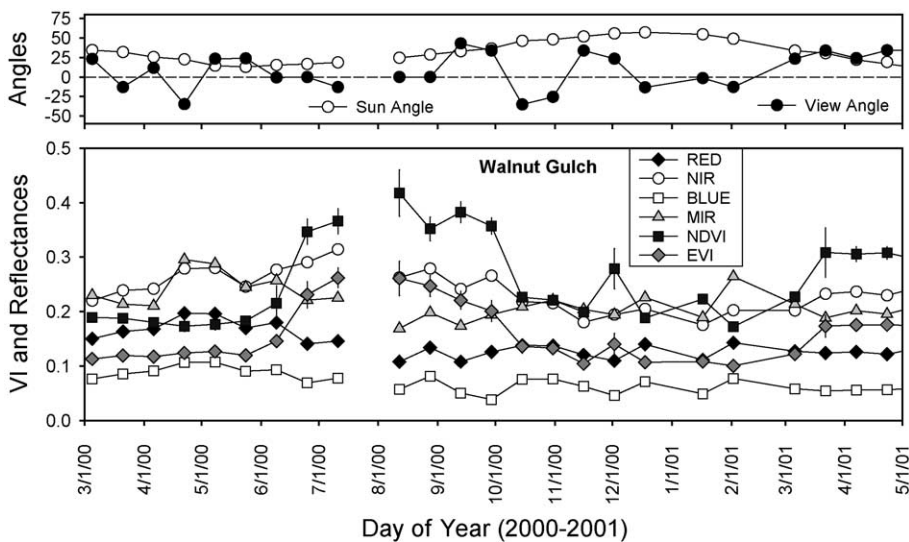


Fig. 9. 1-km MODIS VI and reflectance seasonal profiles, with view and sun angle variability of the selected pixels, at the Walnut Gulch site.

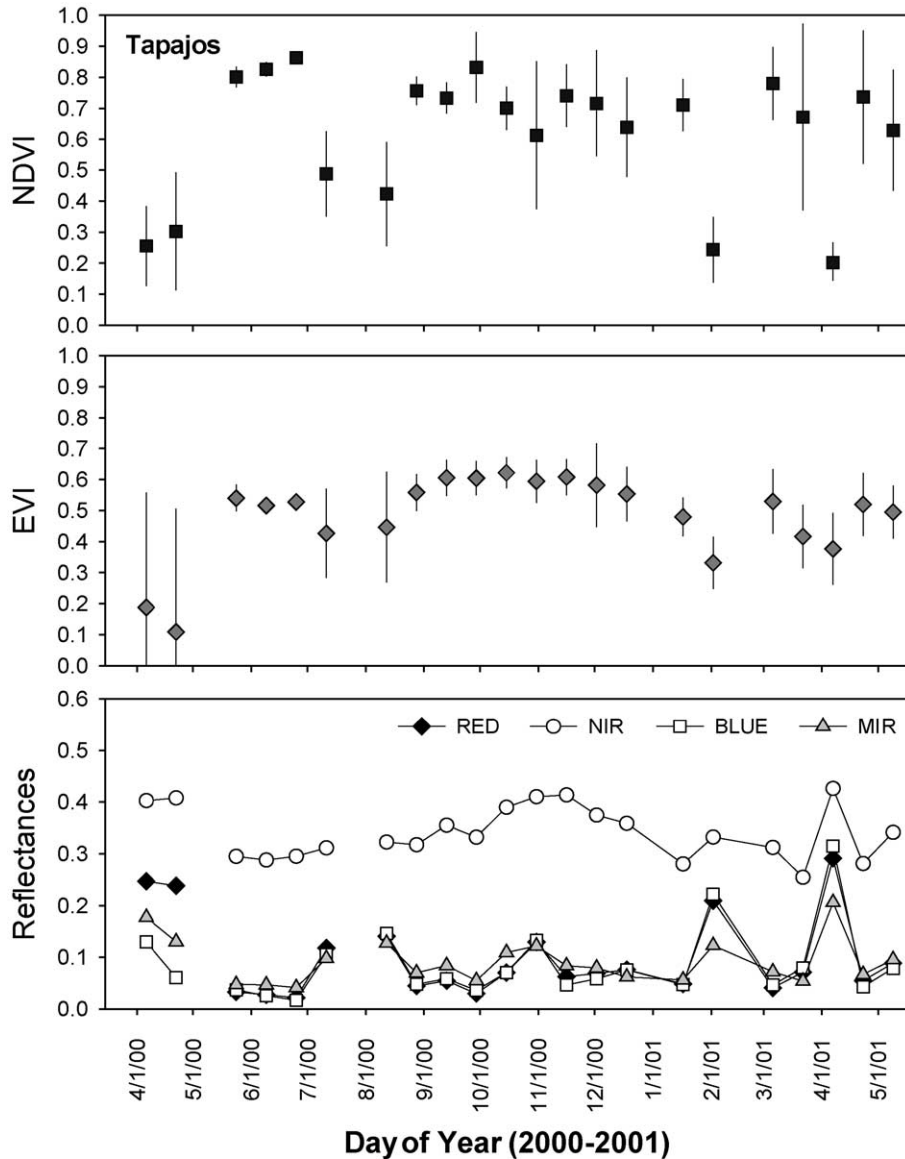


Fig. 10. 1-km MODIS NDVI, EVI, and reflectance seasonal profiles at the Tapajos Forest site.

phenology events, such as onset of greenness (early June), peak greenness (August), and the dry down period (September). The NIR reflectances followed the seasonal dynamics while the blue, red, and MIR reflectances were more variable and appeared to shift to their lowest values after the peak growing season period (Fig. 9). View angle variations were of equivalent magnitude to those encountered at the Konza Prairie grassland site ( $\pm 30^\circ$ ).

The temporal profiles at the Tapajos Amazon Forest site showed no strong phenology patterns (Fig. 10). This site is characterized as seasonal tropical forest with an annual rainfall of about 2200 mm with overstory PAI values in the 5–7 range and a fairly closed canopy cover usually exceeding 90%. There is a slight increase in EVI values in the late dry season (October–December) which may be related to the herbaceous understory (Fig. 10). This is also seen in the increase in NIR reflectances for the same period

while the blue, red, and MIR reflectances are mostly below 0.10 and consistent throughout the year. The sudden increase in blue and red reflectances to values slightly higher than MIR reflectance in July and August 2000 is documented in the QA results as residual cloud contamination. The compositing routine selected these contaminated pixels because they were the best observations over their 16-day periods. The contaminated pixels exhibited degraded NDVI values and less pronounced decreases in the EVI. The VIs and reflectance values exhibited strong view-angle related fluctuations with the NDVI showing the most view angle variability and reflectances showing the least. These variations resulted in significant ‘noise’ that inhibited the utility of the VIs for studies on Amazon forest seasonality patterns.

A set of multitemporal seasonal profiles of 1-km, 16-day MODIS VI composites are shown in Fig. 11 for a wide

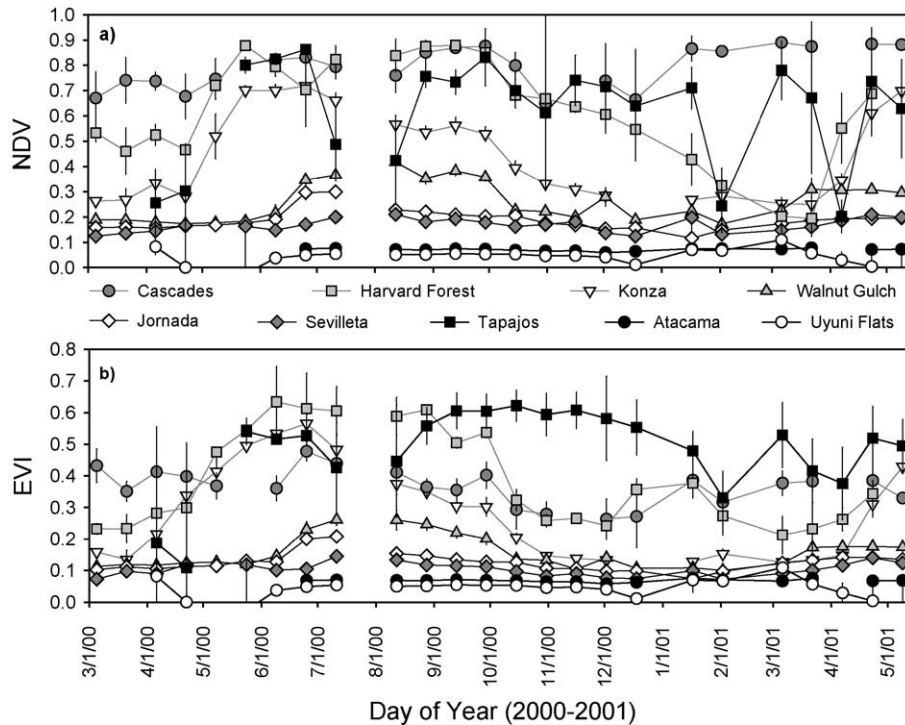


Fig. 11. 1-km MODIS NDVI and EVI seasonal profiles over a wide range of biomes.

range of biomes, including hyperarid sites, semi-arid to humid grassland sites, and forest sites. The hyperarid sites provided a baseline measure of near-zero vegetation. The dynamic range for all the sites varied from  $\sim 0.05$  to nearly 0.9 for the NDVI with the broadleaf Harvard Forest producing the highest values followed by the needleleaf forest in the Cascades, the Tapajos Forest, Konza Prairie, the Arizona semi-arid grassland sites, the drier New Mexico grass-shrub sites, and the hyperarid Uyuni and Atacama sites (Fig. 11a). There was little differentiation between the needleleaf and broadleaf forests in the growing season. Maximum contrast among all the sites occurred during the summer growing season when all of the sites became separable, based on their NDVI values.

The MODIS EVI seasonal profiles also depicted the growing season of the various biomes fairly well (Fig. 11b). The dynamic range of EVI values over these sites varied from 0.05 to 0.65, a smaller dynamic range than that of the NDVI. The Tapajos and Harvard forest sites had the highest EVI values, followed by Konza Prairie, the needleleaf Cascade forest site, the Arizona sites, the New Mexico sites, and then the hyperarid sites. The EVI exhibited a well-defined Konza Prairie peak with higher overall contrast and symmetry from dry to wet season. Overall, the EVI seasonal curves appeared more symmetrical about the peak of the growing season than encountered with the NDVI. There was a strong contrast in EVI values between broadleaf and needleleaf forests which would be useful in discrimination and mapping forest types. The two hyperarid sites presented nonvegetation related variations in both VIs. This bare soil

noise results from the wide range of soil spectral variations in arid regions and define a lower threshold of vegetation detection.

The net effect of the sun/view angle geometries of the selected pixels in the MODIS composites was only a slight bias toward the forward scatter direction, which encompassed 60% of the pixels selected and shown in Fig. 11. The CV-MVC procedure selected pixels to within  $\pm 30^\circ$  sensor view angles where 87% of the pixels fell. A total of 55% of the pixels fell within  $\pm 20^\circ$  sensor view angles, and 34% of the pixels fell to within  $\pm 10^\circ$  viewing angles. Nevertheless, this was the major source of noise present in the seasonal time series data presented here. View angle influences certainly degrade the seasonal profiles and impact on accurate assessments of the start of the growing season, the peak of the growing season, and initiation of dry-down period.

Crossplots of the two VIs showed a curvilinear relationship between them, such that the NDVI always had higher values but appeared to reach an asymptotic maximum value (Fig. 12). For the semiarid shrub and grassland biomes, the two VIs are well correlated. We can observe major differences and separate relationships for the grassland, forested, and shrub biomes as well as for bare soil. For the forests, there were significant differences and the two VIs were not well correlated. A separate relationship appears for the hyperarid sites (Uyuni and Atacama), the semi-arid sites (Walnut Gulch, Sevilleleta, and Jornada), the grassland site (Konza), and the forested sites (Tapajos, Harvard, and Cascades) (Fig. 12). These differences are associated with

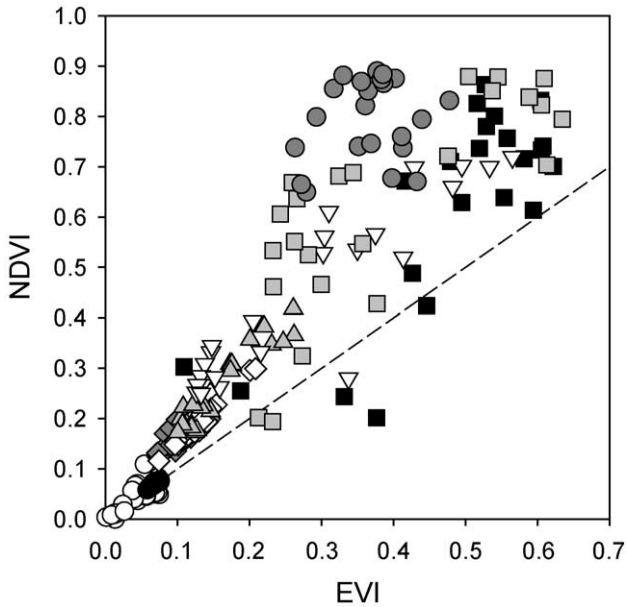


Fig. 12. Crossplot of NDVI and EVI seasonal data for the wide range of biome sites (symbols the same as in Fig. 11).

canopy structural differences within these biome types (Gao, et al., 2000). Values below the 1:1 line in Fig. 12 represent poor quality and contaminated pixels as observed in Fig. 11.

### 4.3. Comparison of MODIS- and AVHRR-NDVI seasonal profiles

A major goal of satellite remote sensing is to observe land surface conditions over long periods of time. Long-term time series observations require much effort to ensure continuity, particularly across new sensors with varying bandpasses and associated target-atmospheric effects, drifts in calibration, and filter degradation. There is the dilemma of maintaining data continuity and a stable time series data record while taking advantage of ‘state of the art’ technology advancements (better sensor properties and band configurations) and improved scientific algorithms. Both the NOAA-AVHRR as well as Landsat sensors offer historical vegetation index time series data going back to the 1970s. We analyzed and compared a 1-year seasonal time series of 1-km MODIS NDVI with an equivalent 1-km AVHRR-NDVI over various North American sites (Fig. 13). The MODIS and AVHRR sensors have widely differing bandpasses with narrower MODIS red and NIR bands (620–670; 841–876 nm) relative to those of the AVHRR (570–700; 710–980 nm). Differences in bandpasses may result in dissimilar reflectances and thus, sensor-dependent NDVI values.

In our analysis, the MODIS- and AVHRR-NDVI products depicted the seasonal patterns and phenologies of the wide range of biomes quite well (Fig. 13). During the dry

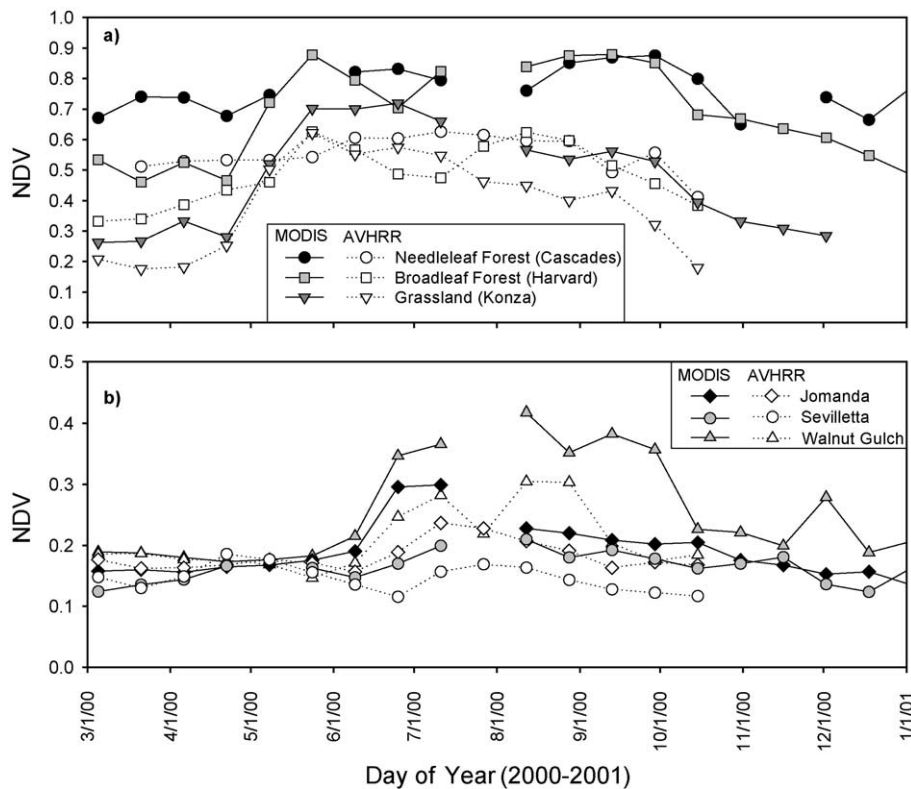


Fig. 13. Comparison of 1-km MODIS and 1-km AVHRR seasonal profiles over (a) a range of North American humid sites and (b) a range of North American semiarid sites.

season, the two NDVI products mimicked each other with nearly identical values over the arid and semi-arid sites (Fig. 13b). However, during the wet growing season period, the MODIS-NDVI values were significantly higher than those from the AVHRR resulting in a greater seasonal dynamic range for each site. Sensor-induced, NDVI differences were greater over the more humid sites with the greatest discrepancies over the wet growing season (Fig. 13a). The MODIS-NDVI exhibited greater sensitivity and separation among the humid grassland (Konza), broadleaf (Harvard), and needleleaf forests (Cascades) during the peak of the growing season compared with the AVHRR-NDVI values (Fig. 13a).

A major cause of these differences can be attributed to the influence of water vapor content in the atmosphere, which strongly affected the AVHRR-NIR band and caused NDVI values to decrease, especially in the humid wet season (Cihlar, Tcherednichenko, Latifovic, Li, & Chen, 2001; Justice, Eck, Tanre, & Holben, 1991). The narrower MODIS-NIR band avoids the water absorption regions of the spectrum and was nearly unaffected by the seasonal variations in atmospheric water vapor contents. An NDVI crossplot from the two sensors show the difficulties in a simple translation between the two datasets for NDVI continuity purposes (Fig. 14). The overall slope of the MODIS-AVHRR crossplot is 1.45 with significant atmosphere-induced scatter. The AVHRR-NDVI dynamic range for this extracted seasonal data set was 0.12 to 0.62 (0.50 difference) while the equivalent dynamic range for the MODIS NDVI was 0.12 to 0.88 (0.76 difference), or 50% higher.

The higher sensitivity and fidelity of the MODIS-NDVI may also be partly attributed to increased chlorophyll

sensitivity in the MODIS-red band (Gitelson & Kaufman, 1998). There are other differences between the NDVI data sets from the two sensors, including the compositing method and period. The MODIS product is a 16-day composite while the AVHRR data are composited over 14 days. The MODIS data was composited with the constrained view angle, CV-MVC, while the MVC method was used to generate the AVHRR-NDVI product (James & Kalluri, 1994). Both MODIS and AVHRR-NDVI products were corrected for Rayleigh scattering and ozone absorption, however, the MODIS version also received a climatology-based aerosol correction.

#### 4.4. Dynamic range and saturation

Generally, vegetation indices approach a saturation level asymptotically in high biomass regions and for a certain range of LAI (Sellers, 1985). Saturation effects have important consequences for change detection and land use conversion monitoring. We explored the issue of dynamic range and saturation with an analysis of 250-m, 500-m, and 1-km MODIS NDVI and EVI, over a steep climatic gradient encompassing the hyperarid Atacama desert (no vegetation), the semi-arid and sub-humid portions of the Brazilian cerrado (savanna biome), and the humid and perhumid portions of the Amazon tropical rainforest (Fig. 15). This area encompassed a large portion of South America with an LAI range of 0 (Atacama) to approximately 8 (perhumid Amazonia). The histogram of NDVI values is relatively structureless with a narrow forest peak at NDVI~0.85. The peak has a sharp right hand shoulder indicative of saturation. By contrast, the EVI histogram contains a more normally distributed forest peak (EVI=0.7), a broad cerrado peak (EVI=0.4), and a sharper Atacama desert peak (EVI=0.1). An analyses of the individual band histograms showed that only the 'red' signal had saturated while the NIR signal had a normal distribution and was able to depict canopy variations (Fig. 15). The MODIS EVI relies on the nonsaturated NIR band to detect vegetation variations in high biomass areas.

The MODIS-VI values were also plotted along with the MQUALS-ASD results obtained over the Brazilian cerrado and Amazon forest (Tapajos site) biomes and land conversion areas (Fig. 16). The airborne ASD reflectances were first convolved to the MODIS bands prior to VI computation. The MQUALS and MODIS data showed a curvilinear relationship between NDVI and EVI, such that NDVI values were always higher than the EVI values. EVI values averaged 0.4 in the drier cerrado region with corresponding NDVI values at 0.7. The difference between NDVI and EVI values decreased in the primary and regeneration (secondary) forest sites with EVI values approaching 0.8 while the NDVI became asymptotic at ~0.9. The finer spatial resolution MQUALS VI data (~40 m diameter) was able to depict more variations and heterogeneity within the individual biome types. The

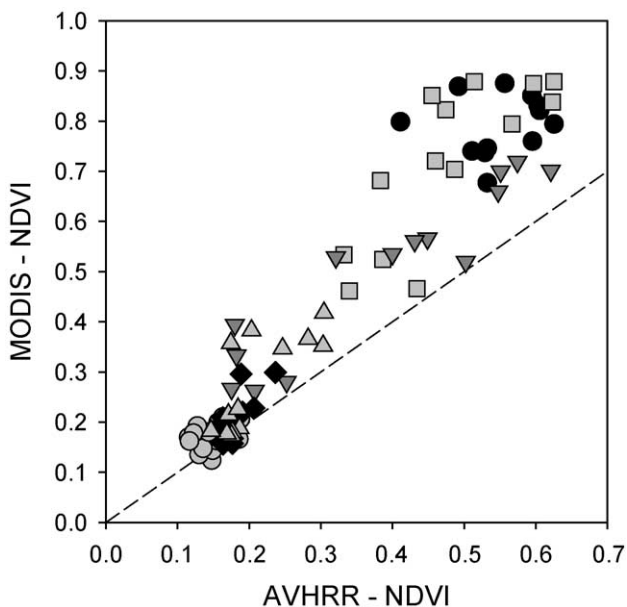


Fig. 14. Crossplot of MODIS and AVHRR-derived NDVI products over the 2000 growing season (symbols the same as in Fig. 13).

### 250m, 16-days composite, Sept. 29-Oct. 14, 2000

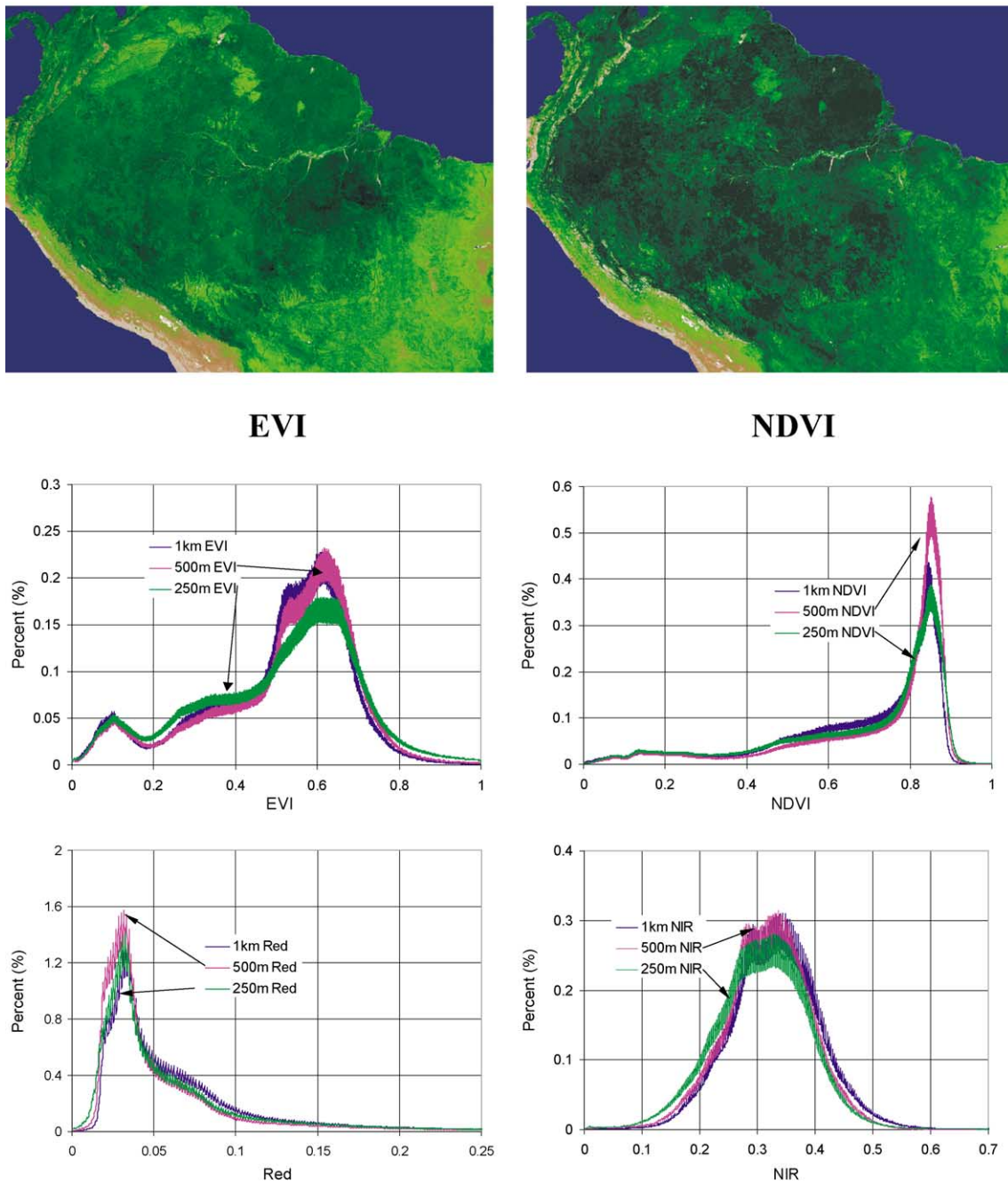


Fig. 15. Histogram structures of 250-m, 500-m, and 1-km MODIS NDVI and EVI over South America spanning the Atacama desert to the Amazon forest.

number of MODIS pixels within a validation area was limited and each 500-m pixel averaged much of the spatial variance within a validation site.

The ASD-derived EVI values showed maximum values at approximately 0.75 in contrast to the lower values derived from coarser resolution MODIS data (0.60). The maximum NDVI values were approximately the same in both the MQUALS and MODIS data (0.90), indicating the upper limit had been reached (Fig. 16). NDVI and EVI

values derived from canopy radiant transfer models over a series of biome types also produced corresponding NDVI and EVI values of 0.90 and 0.75, respectively (Gao, et al., 2000). The dense green pastures within the Tapajos site exhibited a different NDVI-EVI behavior (Fig. 16). The pasture site had equivalent EVI values as the forested areas and equivalent NDVI values as the cerrado areas. The relatively small size of the pasture sites made it too difficult to extract MODIS pixels for this study, however, it

appeared that the use of multiple VIs would ensure separation of these land cover types.

4.5. Biophysical relationships

Vegetation indices have been correlated with various vegetation parameters such as LAI, biomass, canopy cover, and fAPAR. LAI is closely related to a variety of canopy processes, such as interception, evapotranspiration, and leaf litterfall while fAPAR is an important variable in studies of the carbon cycle and energy budget of the vegetated land surface. The VI approach towards biophysical parameter extraction generally employs empirical relationships that are land cover and parameter specific. Many studies have found VI to LAI/fAPAR relationships to be canopy structure- and land cover-dependent, varying with leaf angle distribution, vegetation clumping, and the optical properties of leaf and branch canopy components (Baret & Guyot, 1991; Bégué, 1993; Goward & Huemmrich, 1992). Different canopy types and structures exhibit large variations in reflectance properties, which can produce different VI values for similar LAI and fAPAR conditions. This demonstrates the non-uniqueness of the VIs (Pinty, Leprieur, & Verstraete, 1993) and suggests the need to integrate specific land cover information to derive biophysical parameters from VIs.

A complete biophysical analysis and validation of the MODIS VIs are beyond the scope of this study. Preliminary results from aggregation of LAI field measurements with MODIS 1-km data for a diverse group of vegetation physiognomies are presented in Fig. 17. Although this only involves a limited number of points, it does show that both VIs correlate and respond positively to increases in LAI and PAI. Both VIs appeared to respond well to the high PAI values encountered in the Tapajos rainforest (LAI~6.5); however, many LAI measurements co-registered with a lot more individual MODIS pixels would be needed to assess to

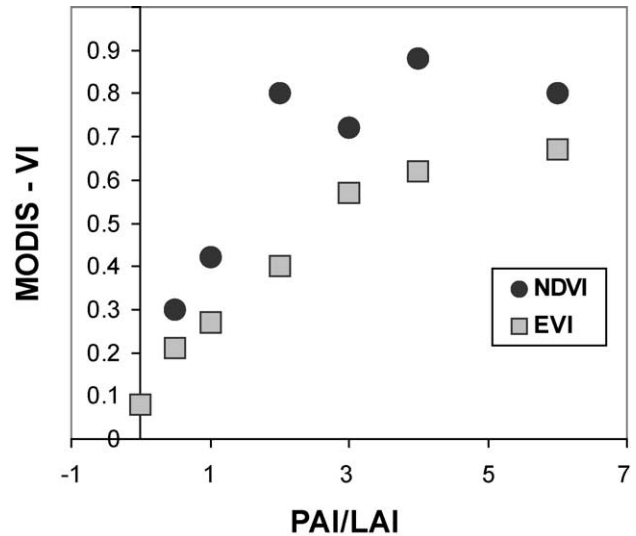


Fig. 17. Relationship between field-based biophysical PAI/LAI data with MODIS sensor data over a wide range of validation test sites.

what extent the VIs are able to depict actual variations in LAI at these high vegetation densities.

5. Discussion and conclusions

In this preliminary performance and validation study, we demonstrated the utility of the MODIS VI products in providing useful radiometric and biophysical information for land surface characterization. Four validation test sites were sampled in a consistent manner with an identical and ‘traceable’ MQUALS radiometric package. In conjunction with simultaneous field sampling, MQUALS allowed us to collect a self-contained set of biophysical and radiometric data from the same ground pixels, which was correlated and compared with MODIS pixel values.

The MODIS-VIs were found to be sensitive to multi-temporal (seasonal) vegetation variations, land cover variations, and biophysical parameter variations. Both the NDVI and EVI demonstrated a good dynamic range and sensitivity for monitoring and assessing spatial and temporal variations in vegetation amount and condition. The ranges in NDVI and EVI values for each biome type showed the NDVI to have a higher range in values over the semiarid sites, but at the expense of a lower dynamic range over the more humid forested sites. Both VIs had an identical range in values for the intermediate mesic grassland site. The lower EVI values found over all the biomes examined is necessary to avoid the ‘saturation’ effects encountered in the NDVI (see Fig. 16). Further studies are needed to define the upper limit of EVI values, which in the case of the NDVI was clearly defined at approximately 0.90.

The MODIS-NDVI seasonal profiles were more sensitive and performed with greater fidelity than the equivalent AVHRR-NDVI profiles, particularly in atmospheres with

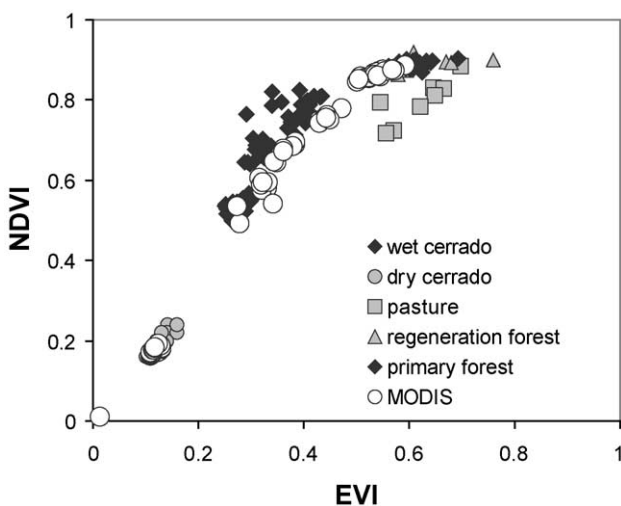


Fig. 16. Crossplots of MQUALS and 500-m MODIS NDVI and EVI data obtained over the Tapajos Forest and Brasilia cerrado validation sites.

high water vapor contents which strongly depressed the AVHRR-NIR channel. However, the increased sensitivity of the MODIS VIs to the land surface also resulted in greater view angle variations from anisotropic vegetated canopies. As a result, most of the noise in the 16-day MODIS composites were attributable to sensor view angle effects with some noise from residual cloud and aerosol contamination. The consequences of compositing-related noise include misclassification of such parameters as onset of greenness, peak of the growing season, length of the growing season, characterization of the dry down period for carbon studies, inter-annual comparisons of phenology, and estimates of net primary production based on integrated temporal VI profiles.

The BRDF-module in the MODIS compositing routine should minimize the angular variations in the VI; however, the BRDF technique was successful in only limited areas due to the difficulty in attaining the required five clear views over the 16-day compositing period for model inversion. Since vegetation is most active during the rainy (cloudy) season, especially in arid and semiarid regions, the optimal selection of clear and representative pixels is greatly impeded by residual clouds in the compositing methodology. The CV-MVC successfully reduced the view angles of pixel acquisitions to within  $\pm 30^\circ$ , which was an improvement over the simple selection of maximum NDVI values (MVC). More analyses are needed, however, to determine if the view angles of the selected pixels can be further constrained closer to nadir view. One option is to utilize the 1-km MODIS BRDF product for view angle normalization, but the MODIS-VI products are at a finer resolution (250 and 500 m) and the MODIS BRDF product often requires a month of data to achieve the best results, whereas the MODIS-VI is 16 days. One can also conduct post-season processing and cleaning of the MODIS multi-temporal profiles, but this has the disadvantage of altering 'measured' VI values based on statistical, not physical, criteria.

Regardless of the composite methodology used, maximum errors are expected when only a single pixel, which could be from any sensor view angle, is available over a compositing cycle. In this situation, strong discontinuities may be present between adjacent pixels acquired on different days and with different view angles. Every composite cycle will have variable results since selected pixels are not consistent to specific viewing geometries and are highly dependent on unpredictable cloud activity. The use of nadir-looking MQUALS as well as nadir-looking satellite sensors, such as ETM+, provide a check on how well the MODIS compositing algorithm is approximating standard nadir-view VIs. When Landsat ETM+ has a cloud-free view of a pixel then so should MODIS, given their formation flying minutes apart.

Much effort has been devoted to improving the NDVI as well as in developing new VIs, resulting in optimized VIs for vegetation monitoring studies. Some of the relevant

features of improved VIs include decreased sensitivity to atmospheric aerosol conditions, lower sensitivity to vegetation canopy background variations (wet, dry, snow, litter), and extended linearity to biophysical parameters over a wide range of vegetation conditions. Reduction of 'saturation' effects and improved linearity adds to the observed accuracy in estimating biophysical parameters from the VI values and provides a mechanism for multi-sensor (resolution) scaling of VI values. The atmosphere and soil resistance capability in optimized VIs provides the capability to produce comparable VI products across different sensors (continuity) and will result in more stable vegetation measures with increased fidelity for change detection and monitoring.

Although our very limited results showed the MODIS VIs to be well correlated with LAI across a range of canopy structure types and species lifeforms, the use of VIs for biophysical parameter retrievals is a challenging task and there remains much work in understanding VI sensitivities across and within biomes. VIs represent an integrative measure of both vegetation photosynthetic activity and canopy structural variations that is useful in monitoring, time series analysis, and change detection studies (inter-annual and seasonal). Spatial and temporal variability in VIs arise from several vegetation related properties, including LAI, canopy structure/architecture, species composition, land cover type, leaf optics, canopy crown cover, understory vegetation, and green biomass. At regional and global scales, these vegetation parameters simultaneously change and one needs to separate such effects before being able to confidently use the VIs to extract a single parameter. Validation test sites are necessary in this respect and provide valuable global "markers" useful in VI interpretations and analyses.

## Acknowledgements

This work is supported by NASA/MODIS Contract no. NAS5-31364. We thank Hiroki Yoshioka, Karim Batchily, Fricky Keita, and Hugo Rodriguez in helping with field and airborne data collection.

## References

- Asrar, G., Fuchs, M., Kanemasu, E. T., & Hatfield, J. L. (1984). Estimating absorbed photosynthetic radiation and leaf area index from spectral reflectance in wheat. *Agronomy Journal*, 76, 300–306.
- Baret, F., & Guyot, G. (1991). Potentials and limits of vegetation indices for LAI and APAR assessment. *Remote Sensing of Environment*, 35, 161–173.
- Bégué, A. (1993). Leaf area index, intercepted photosynthetically active radiation, and spectral vegetation indices: a sensitivity analysis for regular-clumped canopies. *Remote Sensing of Environment*, 46, 45–59.
- Cihlar, J., Ly, H., Li, Z., Chen, J., Pokrant, H., & Huang, F. (1997). Multi-temporal, multichannel AVHRR data sets for land biosphere studies: artifacts and corrections. *Remote Sensing of Environment*, 60, 35–57.

- Cihlar, J., Manak, D., & Voisin, N. (1994). AVHRR bidirectional reflectance effects and compositing. *Remote Sensing of Environment*, 48, 77–88.
- Cihlar, J., Tcherednichenko, I., Latifovic, R., Li, Z., & Chen, J. (2001). Impact of variable atmospheric water vapor content on AVHRR data corrections over land. *IEEE Transactions on Geoscience and Remote Sensing*, 39, 173–180.
- Crist, E. P., & Cicone, R. C. (1984). A physically based transformation of Thematic Mapper data—the TM Tasseled Cap. *IEEE Transactions on Geoscience and Remote Sensing*, GE-22, 256–263.
- Gao, X., Huete, A. R., Ni, W., & Miura, T. (2000). Optical–biophysical relationships of vegetation spectra without background contamination. *Remote Sensing of Environment*, 74, 609–620.
- Gitelson, A., & Kaufman, Y. (1998). MODIS NDVI optimization to fit the AVHRR data series—spectral consideration. *Remote Sensing of Environment*, 66, 343–350.
- Goward, S. N., Markham, B., Dye, D. G., Dulaney, W., & Yang, J. (1991). Normalized difference vegetation index measurements from the Advanced Very High Resolution Radiometer. *Remote Sensing of Environment*, 35, 257–277.
- Goward, S. N., & Huemmrich, K. F. (1992). Vegetation canopy PAR absorption and the normalized difference vegetation index: an assessment using the SAIL model. *Remote Sensing of Environment*, 39, 119–140.
- Graetz, R. D. (1990). Remote sensing of terrestrial ecosystem structure: an ecologist's pragmatic view. In R. J. Hobbs, & H. A. Mooney (Eds.), *Remote sensing of biosphere functioning* (pp. 5–30). New York: Springer-Verlag.
- Holben, B. N. (1986). Characterization of maximum value composites from temporal AVHRR data. *International Journal of Remote Sensing*, 7, 1417–1434.
- Huete, A. R. (1988). A soil-adjusted vegetation index (SAVI). *Remote Sensing of Environment*, 25, 295–309.
- Huete, A., et al (1999). A light aircraft radiometric package for MODLand Quick Airborne Looks (MQUALS). *Earth Observations*, 11, 22–25 (NASA/GSFC).
- Huete, A., Justice, C., & Liu, H. (1994). Development of vegetation and soil indices for MODIS-EOS. *Remote Sensing of Environment*, 49, 224–234.
- Huete, A. R., Liu, H. Q., Batchily, K., & van Leeuwen, W. J. D. (1997). A comparison of vegetation indices over a global set of TM images for EOS-MODIS. *Remote Sensing of Environment*, 59, 440–451.
- James, M. E., & Kalluri, S. N. V. (1994). The pathfinder AVHRR land data set: an improved coarse resolution data set for terrestrial monitoring. *International Journal of Remote Sensing*, 15, 3347–3363.
- Justice, C., Belward, A., Morisette, J., Lewis, P., Privette, J., & Baret, F. (2000). Developments in the 'validation' of satellite sensor products for the study of the land surface. *International Journal of Remote Sensing*, 21, 3383–3390.
- Justice, C. O., Eck, T. F., Tanre, D., & Holben, B. (1991). The effect of water vapor on the normalized difference vegetation index derived for the Sahelian region from NOAA AVHRR data. *International Journal of Remote Sensing*, 12, 1165–1187.
- Justice, D. H., Salomonson, V., Privette, J., Riggs, G., Strahler, A., Lucht, R., Myneni, R., Knjazihhin, Y., Running, S., Nemani, R., Vermote, E., Townshend, J., Defries, R., Roy, D., Wan, Z., Huete, A., van Leeuwen, R., Wolfe, R., Giglio, L., Muller, J.-P., Lewis, P., & Barnsley, M. (1998). The Moderate Resolution Imaging Spectroradiometer (MODIS): land remote sensing for global change research. *IEEE Transactions on Geoscience and Remote Sensing*, 36, 1228–1249.
- Kaufman, Y. J., & Tanré, D. (1992). Atmospherically resistant vegetation index (ARVI) for EOS-MODIS. *IEEE Transactions on Geoscience and Remote Sensing*, 30, 261–270.
- Kimes, D. S. (1983). Dynamics of directional reflectance factor distribution for vegetation canopies. *Applied Optics*, 22, 1364–1372.
- Miura, T., Huete, A. R., van Leeuwen, W. J. D., & Didan, K. (1998). Vegetation detection through smoke-filled AVIRIS images: an assessment using MODIS band passes. *Journal of Geophysical Research*, 103, 32001–32011.
- Miura, T., Huete, A. R., Yoshioka, H., & Holben, B. N. (2001). An error and sensitivity analysis of atmospheric resistant vegetation indices derived from dark target-based atmospheric correction. *Remote Sensing of Environment*, 78, 284–298.
- Myneni, R. B., Keeling, C. D., Tucker, C. J., Asrar, G., & Nemani, R. R. (1997). Increased plant growth in the northern high latitudes from 1981 to 1991. *Nature*, 386, 698–702.
- Peterson, D. L., Aber, J. D., Matson, P. A., Card, D. H., Swanberg, N., Wessman, C., & Spanner, M. (1988). Remote sensing of forest canopy and leaf biochemical contents. *Remote Sensing of Environment*, 24, 85–108.
- Pinty, B., Leprieux, C., & Verstraete, M. M. (1993). Towards a quantitative interpretation of vegetation indices, part I: biophysical canopy properties and classical indices. *Remote Sensing of Environment*, 7, 127–150.
- Potter, C. S., Klooster, S. A., & Brooks, V. (1999). Interannual variability in terrestrial net primary production: exploration of trends and controls on regional to global scales. *Ecosystems*, 2, 36–48.
- Richardson, A. J., & Wiegand, C. L. (1977). Distinguishing vegetation from soil background information. *Photogrammetric Engineering and Remote Sensing*, 43, 1541–1552.
- Roderick, M., Smith, R., & Lodwick, G. (1996). Calibrating long-term AVHRR-derived NDVI imagery. *Remote Sensing of Environment*, 58, 1–12.
- Running, S. W., Justice, C., Salomonson, V., Hall, D., Barker, J., Kaufman, Y., Strahler, A., Huete, A., Muller, J. P., Vanderbilt, V., Wan, Z. M., Teillet, P., & Carneggie, D. (1994). Terrestrial remote sensing science and algorithms planned for EOS/MODIS. *International Journal of Remote Sensing*, 15, 3587–3620.
- Schlesinger, W. H., Reynolds, J. F., Cunningham, G. L., et al (1990). Biological feedback in global desertification. *Science*, 247, 1043–1048.
- Sellers, P. C. (1985). Canopy reflectance, photosynthesis and transpiration. *International Journal of Remote Sensing*, 6, 1335–1372.
- Tucker, C. J. (1979). Red and photographic infrared linear combinations for monitoring vegetation. *Remote Sensing of Environment*, 8, 127–150.
- Tucker, C. J., Townshend, J. R. G., & Goff, T. E. (1985). African land-cover classification using satellite data. *Science*, 227, 369–375.
- van Leeuwen, W. J. D., Huete, A. R., & Laing, T. W. (1999). MODIS vegetation index compositing approach: a prototype with AVHRR data. *Remote Sensing of Environment*, 69, 264–280.
- Vermote, E., El Saleous, N., & Justice, C. (2002). Atmospheric correction of the MODIS data in the visible to middle infrared: First results. *Remote Sensing of Environment*, 83, 97–111 (this issue).
- Verstraete, M. M., & Pinty, B. (1996). Designing optimal spectral indexes for remote sensing applications. *IEEE Transactions on Geoscience and Remote Sensing*, 34, 1254–1265.
- Walthall, C. L., Norman, J. M., Welles, J. M., Campbell, G., & Blad, B. L. (1985). Simple equation to approximate the bidirectional reflectance from vegetative canopies and bare soil surfaces. *Applied Optics*, 24, 383–387.